Article

Hydrogen Generation from Weak Acids: Electrochemical and Computational Studies of a Diiron Hydrogenase Mimic

Greg A. N. Felton, Aaron K. Vannucci, Jinzhu Chen, L. Tori Lockett, Noriko Okumura, Benjamin J. Petro, Uzma I. Zakai, Dennis H. Evans, Richard S. Glass, and Dennis L. Lichtenberger

J. Am. Chem. Soc., **2007**, 129 (41), 12521-12530• DOI: 10.1021/ja073886g • Publication Date (Web): 26 September 2007

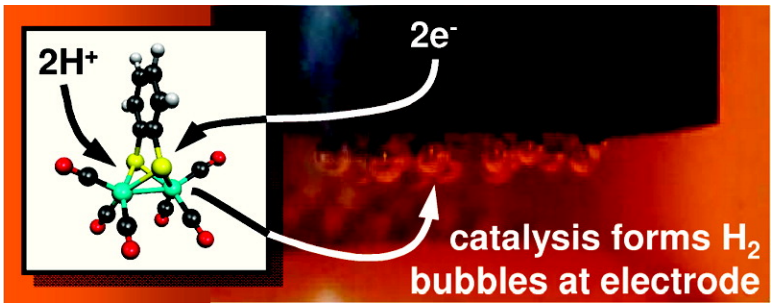

More About This Article

Additional resources and features associated with this article are available within the HTML version:

- Supporting Information
- Links to the 11 articles that cite this article, as of the time of this article download
- Access to high resolution figures
- Links to articles and content related to this article
- Copyright permission to reproduce figures and/or text from this article

View the Full Text HTML

J|A|C|S
ARTICLES
Published on Web 09/26/2007

Hydrogen Generation from Weak Acids: Electrochemical and Computational Studies of a Diiron Hydrogenase Mimic

Greg A. N. Felton,† Aaron K. Vannucci, Jinzhu Chen,‡ L. Tori Lockett, Noriko Okumura, Benjamin J. Petro, Uzma I. Zakai, Dennis H. Evans,* Richard S. Glass,* and Dennis L. Lichtenberger*

Contribution from the Department of Chemistry, The University of Arizona, Tucson, Arizona 85721

Received May 30, 2007; E-mail: dhevans@email.arizona.edu; rglass@email.arizona.edu; dlichten@email.arizona.edu

Abstract: Extended investigation of electrocatalytic generation of dihydrogen using [(μ-1,2-benzenedithiolato)][$Fe(CO)_3$]$_2$ has revealed that weak acids, such as acetic acid, can be used. The catalytic reduction producing dihydrogen occurs at approximately −2 V for several carboxylic acids and phenols resulting in overpotentials of only −0.44 to −0.71 V depending on the weak acid used. This unusual catalytic reduction occurs at a potential at which the starting material, in the absence of a proton source, does not show a reduction peak. The mechanism for this process and structures for the intermediates have been discerned by electrochemical and computational analysis. These studies reveal that the catalyst is the monoanion of the starting material and an ECEC mechanism occurs.

Introduction

Hydrogenase enzymes very efficiently catalyze the reductive generation and oxidative uptake of molecular hydrogen.[1] Consequently, simpler catalysts based on these enzymes have been studied.[2−4] The goal is to develop cheap, robust, and reliable catalysts that produce and utilize dihydrogen to empower a future hydrogen energy economy.[5,6] The enzymes typically feature binuclear active sites: either iron and nickel, NiFe hydrogenases or two irons, Fe-only hydrogenases. Models based on the NiFe hydrogenases have recently shown promise.[7] However, catalysts based on the Fe-only hydrogenases have progressed much further. The Fe-only hydrogenases contain an Fe_2S_2 core as their active sites[8−10] as shown schematically in **1**[11] and are especially well-suited for reductive hydrogen generation as shown in eq 1. Furthermore, simple diiron

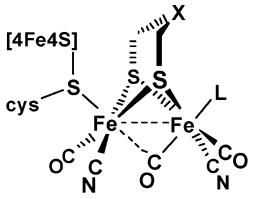

1

$$2H^+ + 2e^- \rightleftharpoons H_2 \qquad (1)$$

complexes analogous to the active site of the enzyme are synthetically accessible, with examples shown in **2**−**5**. Rauch-

† Present address: Department of Chemistry, Princeton University, Princeton, NJ.

‡ Present address: Department of Chemistry, University of Illinois, Urbana, IL.

(1) Frey, M. *ChemBioChem* **2002**, *3*, 153−160.
(2) (a) Darensbourg, M. Y.; Lyon, E. J.; Smee, J. J. *Coord. Chem. Rev.* **2000**, *206*−*207*, 533−561. (b) King, R. B.; Bitterwolf, T. E. *Coord. Chem. Rev.* **2000**, *206*−*207*, 563−579. (c) Darensbourg, M. Y.; Lyon, E. J.; Zhao, X.; Georgakaki, I. P. *Proc. Natl. Acad. Sci. U.S.A.* **2003**, *100*, 3683−3688. (d) Georgakaki, I. P.; Thomson, L. M.; Lyon, E. J.; Hall, M. B.; Darensbourg, M. Y. *Coord. Chem. Rev.* **2003**, *238*−*239*, 255−266. (e) Evans, D. J.; Pickett, C. J. *Chem. Soc. Rev.* **2003**, *32*, 268−275. (f) Liu, X.; Ibrahim, S. K.; Tard, C.; Pickett, C. J. *Coord. Chem. Rev.* **2005**, *249*, 1641−1652. (g) Tard, C.; Liu, X.; Ibrahim, S. K.; Bruschi, M.; De Gioia, L.; Davies, S. C.; Yang, X.; Wang, L.-S.; Sawers, G.; Pickett, C. J. *Nature* **2005**, *433*, 610−613. (h) Sun, L.; Akermark, B.; Ott, S. *Coord. Chem. Rev.* **2005**, *249*, 1653−1663. (i) van der Vlugt, J. I.; Rauchfuss, T. B.; Wilson, S. R. *Chem.*−*Eur. J.* **2006**, *12*, 90−98. (j) Linck, R. C.; Rauchfuss, T. B. In *Bioorganometallics Biomolecules, Labeling, Medicine*; Jaouen, G., Ed.; Wiley-VCH: Weinheim, 2006; Chapter 12. (k) Song, L.-C.; Ge, J.-H.; Zhang, X.-G.; Liu, Y.; Hu, Q.-M. *Eur. J. Inorg. Chem.* **2006**, 3204−3210. (l) Schwartz, L.; Ekström, J.; Lomoth, R.; Ott, S. *Chem. Commun.* **2006**, 4206−4208. (m) Gao, W.; Ekström, J.; Liu, J.; Chen, C.; Eriksson, L.; Weng, L.; Akermark, B.; Sun, L. *Inorg. Chem.* **2007**, *46*, 1981−1991. (n) Wang, Z.; Liu, J.; He, C.; Jiang, S.; Akermark, B.; Sun, L. *Inorg. Chim. Acta.* **2007**, *360*, 2411−2419. (o) Jiang, S.; Liu, J.; Shi, Y.; Wang, Z.; Akermark, B.; Sun, L. *Polyhedron* **2007**, *26*, 1499−1504. (p) Jiang, S.; Liu, J.; Shi, Y.; Wang, Z.; Akermark, B.; Sun, L. *Dalton Trans.* **2007**, 896−902. (q) Duan, L.; Wang, M.; Li, P.; Na, Y.; Wang, N.; Sun, L. *Dalton Trans.* **2007**, 1277−1283. (r) Windhager, J.; Rudolph, M.; Bräutigan, S.; Görls, H.; Weigand, W. *Eur. J. Inorg. Chem.* **2007**, 2748−2760.
(3) Morvan, D.; Capon, J. F.; Gloaguen, F.; Le Goff, A.; Marchive, M.; Michand, F.; Schollhammer, P.; Talarmin, J.; Yaouanc, J. J. *Organometallics* **2007**, *26*, 2042−2052.
(4) Song, L. C.; Yang, Z. Y.; Hua, Y. J.; Wang, H. T.; Liu, Y.; Hu, Q. M. *Organometallics* **2007**, *26*, 2106−2110.
(5) Tye, J. W.; Hall, M. B.; Darensbourg, M. Y. *Proc. Natl. Acad. Sci. U.S.A.* **2005**, *102*, 16911−16912.
(6) Cammack, R.; Frey, M.; Robson, R. *Hydrogen as a Fuel: Learning from Nature*; Taylor & Francis: London, 2001.
(7) (a) Perra, A.; Davies, E. S.; Hyde, J. R.; Wang, Q.; McMaster, J.; Schröder, M. *Chem. Commun.* **2006**, 1103−1105. (b) Oudart, Y.; Artero, V.; Pécaut, J.; Fontecave, M. *Inorg. Chem.* **2006**, *45*, 4334−4336. (c) Ogo, S.; Kabe, R.; Uehara, K.; Kure, B.; Nishimura, T.; Menon, S. C.; Harada, R.; Fukuzumi, S.; Higuchi, Y.; Ohhara, T.; Tamada, T.; Kuroki, R. *Science* **2007**, *316*, 585−587. See also mononuclear Ni catalysts: Wilson, A. D.; Newell, R. H.; McNevin, M. J.; Muckerman, J. T.; Rakowski DuBois, M.; DuBois, D. L. *J. Am. Chem. Soc.* **2006**, *128*, 358−366.
(8) Peters, J. W.; Lanzilotta, W. N.; Lemon, B. J.; Seefeldt, L. C. *Science* **1998**, *282*, 1853−1858.
(9) Nicolet, Y.; Piras, C.; Legrand, P.; Hatchikian, C.; Fontecilla-Camps, J. C. *Struct. Fold Des.* **1999**, *7*, 13−23.
(10) Nicolet, Y.; de Lacey, A. L.; Vernede, X.; Fernandez, V. M.; Hatchikian, C.; Fontecilla-Camps, J. C. *J. Am. Chem. Soc.* **2001**, *123*, 1596−1601.
(11) See ref 5 for further discussion of the diiron structure in the enzyme.

fuss and co-workers[12] reported that **2a** catalyzes reduction of the strong acids: H_2SO_4, HCl, and *p*-toluenesulfonic acid. The first step in this catalysis is protonation of **2a** to give a bridging hydride and an overall CCEE mechanism. Darensbourg and co-workers[13] found that **2b**, **2d**, **3a**, and **4a** electrocatalyze dihydrogen production from the weak acid acetic acid. An EECC mechanism is proposed in which protonation provides a terminal hydride, not bridging. The question of the number of electrons involved in the initial reduction of **2b** has been thoroughly discussed by Borg et al.[14] Electrocatalytic reduction of acetic acid is also reported for **2c**, **3b**, and **4b** by an ECCE or EC mechanism. Song and co-workers[4] reported that **5** catalyzes reduction of Et_3NHCl. Ott and co-workers[15] have also isolated an N-protonated iron hydride complex that may model the Fe-only hydrogenase intermediate leading to molecular hydrogen formation. The number of related molecules being studied for electrocatalytic production of dihydrogen is increasing continually.

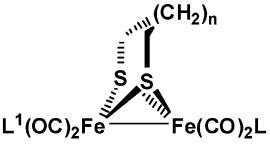

2a: n=1, L=PMe_3, L'=CN^-
b: n=1, L=L'=CO
c: n=1, L=L'=PMe_3
d: n=0, L=L'=CO

3a: L=CO
b: L=PMe_3

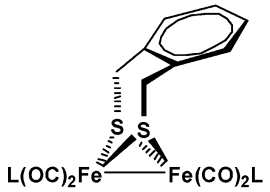

4a: L=CO
b: L=PMe_3

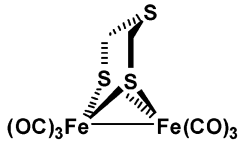

5

Compound **6** has a benzenedithiolate ligand (bdt) bridging the two iron centers to form the Fe_2S_2 core. Enemark, Lichtenberger, and co-workers have studied the electronic structure effects of bdt bound to high-valent, early transition metals as a minimum molecular model of the ene-dithiolate interaction of pyranopterin-dithiolate with the active metal sites of Mo/W enzymes.[16−19] These enzymes catalyze a wide range of oxidation/reduction reactions with a variety of substrates. The ene-dithiolate coordination has a special ability to facilitate these reactions by lowering the potential difference between successive metal oxidation states in the catalytic cycle. This is accomplished by an interaction of the metal orbitals with a combination of the filled sulfur p_π orbitals and the benzene p_π orbitals, which acts to buffer the change in electron density at the metal center as the oxidation state is changed, thus minimizing the changes in electron energies. This buffering is aided by the ability of the ene-dithiolate to adapt its geometry with the metal center to the change in electron configuration. The ene-dithiolate may also serve as an effective electron-transfer pathway. Based on these electronic properties of ene-dithiolates and their use by nature in other metal redox enzymes, it is anticipated that coupling of the bdt ligand with the Fe_2S_2 core in molecules analogous to the active sites of hydrogenases should have significant benefits for the chemistry of these systems.

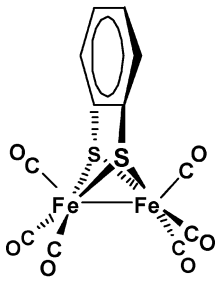

6

Compound **6** has been the subject of two earlier electrochemical studies,[20,21] but neither reported the reduction of protons from weak acids shown here. The principal findings of these studies were as follows. In either dichloromethane or acetonitrile as solvent, **6** is reduced to its dianion in a *reversible two-electron* process with closely spaced individual standard potentials, $E°_1$ and $E°_2$, where $E°_1$ is the standard potential for insertion of the first electron into **6**, $\mathbf{6} + e^- \rightleftharpoons \mathbf{6}^-$, and $E°_2$ is the corresponding standard potential for the second, $\mathbf{6}^- + e^- \rightleftharpoons \mathbf{6}^{2-}$. In comparison, **2b**, which is similar in structure but has only a simple propanedithiolate bridge, undergoes an initial *quasi-reversible one-electron* reduction at about a 0.4 V more negative potential than **6**, and a second *irreversible* reduction of **2b** does not occur until about another 0.6 V more negative potential than the initial reduction.[13] Thus the bdt ligand is able to modulate the potentials between oxidation states in this class of molecules as well as in the high-valent early transition metal complexes studied previously. The bdt ligand also stabilizes the molecule **6** in reduced states. With **6** in the presence of the strong acid $HBF_4 \cdot Et_2O$, the two-electron process became irreversible and there was a small but significant increase in the cathodic peak current indicating that catalytic reduction of the acid was occurring at this potential.[22] Similar results were obtained in acetonitrile[21] where significant catalytic reduction was seen with

(12) Gloaguen, F.; Lawrence, J. D.; Rauchfuss, T. B. *J. Am. Chem. Soc.* **2001**, *123*, 9476−9477.
(13) Chong, D.; Georgakaki, I. P.; Mejia-Rodriguez, R.; Sanabria-Chinchilla, J.; Soriaga, M. P.; Darensbourg, M. Y. *Dalton Trans.* **2003**, 4158−4163.
(14) Borg, S. J.; Behrsing, T.; Best, S. P.; Razavet, M.; Liu, X.; Pickett, C. J. *J. Am. Chem. Soc.* **2004**, *126*, 16988−16999.
(15) Schwartz, L.; Eilers, G.; Eriksson, L.; Gogoll, A.; Lomoth, R.; Ott, S. *Chem. Commun.* **2006**, 520−522.
(16) Joshi, H. K.; Inscore, F. E.; Schirlin, J. T.; Dhawan, I. K.; Carducci, M. D.; Bill, T. G.; Enemark, J. H. *Inorg. Chim. Acta* **2002**, *337*, 275−286.
(17) Joshi, H. K.; Cooney, J. J. A.; Inscore, F. E.; Gruhn, N. E.; Lichtenberger, D. L.; Enemark, J. H. *Proc. Natl. Acad. Sci. U.S.A.* **2003**, *100*, 3719−3724.
(18) Joshi, H. K.; Enemark, J. H. *J. Am. Chem. Soc.* **2004**, *126*, 11784−11785.
(19) Cooney, J. J. A.; Cranswick, M. A.; Gruhn, N. E.; Joshi, H. K.; Enemark, J. H. *Inorg. Chem.* **2004**, *43*, 8110−8118.
(20) Capon, J. F.; Gloaguen, F.; Schollhammer, P.; Talarmin, J. *J. Electroanal. Chem.* **2004**, *566*, 241−247.
(21) Capon, J. F.; Gloaguen, F.; Schollhammer, P.; Talarmin, J. *J. Electroanal. Chem.* **2006**, *595*, 47−52.
(22) It was shown[20] that in dichloromethane **6** is reduced to its dianion in a reversible two-electron process with a half-wave potential of −1.44 V vs ferrocenium/ferrocene in dichloromethane. Potential inversion is usually associated with a significant structural change accompanying one or both of the electron-transfer reactions.[23] The authors suggested that this structural change is a fission of one of the Fe−S bonds as proposed by McKennis and Kyba.[24] The structural change must be reversible to account for the overall electrochemical reversibility that is observed.
(23) Macias-Ruvalcaba, N. A.; Evans, D. H. *J. Phys. Chem. B* **2005**, *109*, 14642−14647.
(24) McKennis, J. S.; Kyba, E. P. *Organometallics* **1983**, *2*, 1249−1251.

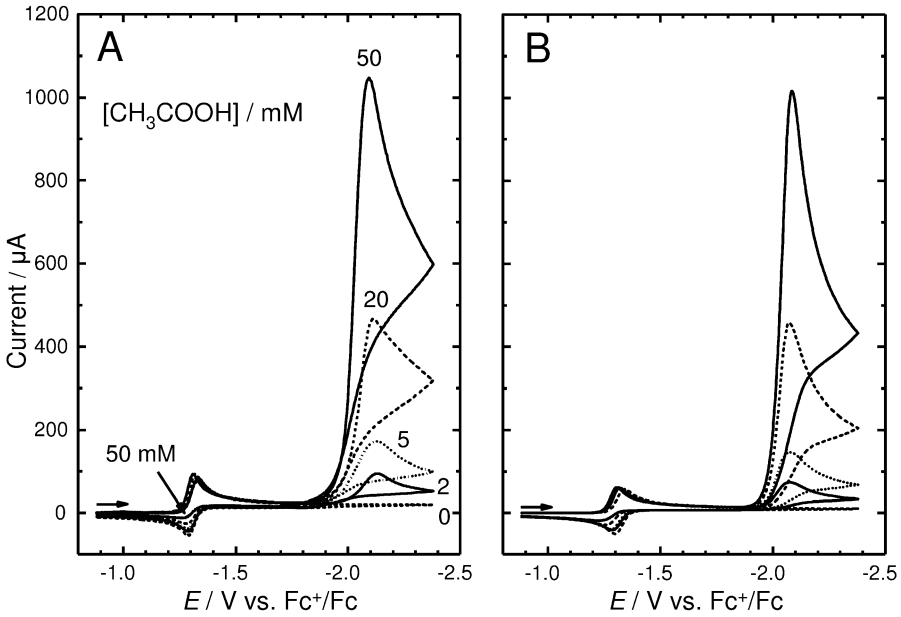

Figure 1. (A) Voltammograms of 1.00 mM **6** in 0.10 M Bu_4NPF_6/CH_3CN at 0.100 V/s in the absence of acetic acid and in the presence of concentrations of acetic acid shown in the figure. (B) Simulation of the voltammograms in Figure 1A using the simulation parameters listed in Table 3.

the somewhat weaker acid, *p*-toluenesulfonic acid ($pK_a = 8.7$ in acetonitrile). The effect of a significantly weaker acid, acetic acid ($pK_a = 22.3$ in acetonitrile), was also studied. No catalysis was observed at the potentials reported, including at the two-electron reduction peak near −1.25 V. This is a required result as it is thermodynamically impossible[25] to reduce an acid at a potential less negative than its standard potential ($E°_{AcOH} = -1.46$ V vs ferrocene[25]). Although catalysis was not observed with acetic acid, the two-electron reduction peak of **6** became irreversible and a new anodic peak was detected. The new anodic peak was assigned to the oxidation of $\mathbf{6H}^-$, formed by protonaton of $\mathbf{6}^{2-}$ by acetic acid.

In the present paper we report a new catalytic reduction of acetic acid that occurs at potentials negative of those studied by Capon et al.[20,21] We have also developed a mechanism for the catalysis by combining electrochemical analysis and theoretical calculations that allows us to successfully match simulations to the experimental data and to determine the rate constant for the rate-limiting step in the catalytic cycle. Finally, we have tested this scheme with other weak acids with pK_a values ranging from 18 to 28 and have found that the same mechanism will account for the results from those acids as well.

Results and Discussion

The new catalytic process for the reduction of acetic acid is illustrated in Figure 1A which shows voltammograms for 1.0 mM **6** in acetonitrile obtained at 0.10 V/s. In the absence of added acid we find the reversible two-electron reduction of **6** reported by Capon et al.[21] When the scan is reversed at −1.5 V in the presence of small concentrations of acetic acid, we see no increase in the reduction peak and suppression of the anodic peak for oxidation of $\mathbf{6}^{2-}$ due to its protonation to form $\mathbf{6H}^-$ just as reported earlier (data not shown).[21] However, when the initial negative-going scan is extended to more negative values in the presence of acetic acid, a peak for the catalytic reduction of acetic acid appears near −2.1 V and its height increases with increasing concentrations of acid (Figure 1A). As will be seen, the overall catalytic rate for the reduction of acetic acid is moderate and depends strongly on the pK_a of the acid being studied. In studies of acetic acid alone, it was shown that direct reduction of acid at the mercury film electrode was negligible in the range of potentials studied. The simulations shown in Figure 1B are discussed below.

To account for the electrocatalytic reduction of a general weak acid HA, it is postulated that protonation of $\mathbf{6}^{2-}$ is the rate-determining step. Thus electrochemical mechanistic studies alone do not provide complete information on subsequent steps. However, insight into the nature of the subsequent steps and the identity of the species involved in catalysis can be obtained from a combination of electrochemical experiments and computational studies. Validation of the computational methods comes from the ability of the computations to account for the geometry, metal-carbonyl stretching frequencies, and electron energies of **6** as well as the reduction potentials and pK_a values of all species in the reaction cycle.

The results for the computed gas-phase structure of **6** are shown in Table 1 and compared with the molecular parameters found by X-ray crystallography.[26] The structural parameters are in close agreement. As another measure of the validity of the computations, the experimental IR spectrum of **6** in the carbonyl stretching region is compared with a simulation based on the geometry optimization and vibrational analysis of the molecule in Figure 2. The calculated carbonyl stretching frequencies are dependent on the electron richness at the metal center and the extent of backbonding to the carbonyls. Also, the calculated splittings and absorption intensities are further dependent on the electronic and dipole coupling between the carbonyls in the normal vibrational modes. The good agreement between the simulated spectrum and the experimental spectrum indicates that the computational method is accounting for the potential energy

(25) Felton, G. A. N.; Glass, R. S.; Lichtenberger, D. L.; Evans, D. H. *Inorg. Chem.* **2006**, *45*, 9181−9184.

(26) Cabeza, J. A.; Martinez-Garcia, M. A.; Riera, V.; Ardura, D.; Garcia-Granda, S. *Organometallics* **1998**, *17*, 1471−1477.

Table 1. Comparison of Computed Structure of **6** to Crystallographic Data[a]

bond/angle	X-ray[b]	DFT[c]
Fe−Fe	2.480	2.474
Fe−S	2.268	2.283
S···S	2.938	2.961
S−C	1.777	1.794
Fe−C[d]	1.792	1.779
C−O[d]	1.135	1.156
S−Fe−S	80.7	80.8
Fe−S−Fe	66.3	65.8
S−Fe−C_a	101.4	102.4
C_a−Fe−C_b	99.8	99.3
C_b−Fe−C_b	91.2	90.2

[a] Bond lengths, Å; angles, degrees. [b] Experimental geometric parameters[26] are averaged to C_{2v} symmetry for the molecule. C_a refers to the apical COs in the local square-based pyramid geometry of each Fe, and C_b refers to the basal COs. [c] See Experimental Section for details of the DFT method. [d] Averaged over all COs.

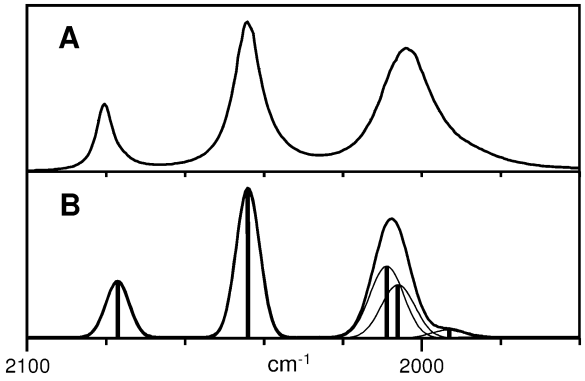

Figure 2. IR spectrum of **6** in the carbonyl stretching region. (A) Experimental. (B) DFT simulation showing individual calculated frequencies and the sum of broadened absorptions (see Experimental Section).

and structure of the molecule as a function of these vibrational distortions very well.

In addition to the ability to account for the structure and dynamics of the neutral molecule, it is particularly important for the computations to be able to account for the energies and structures associated with oxidation and reduction. For the case of oxidation of the neutral molecule, photoelectron spectroscopy provides a precise measure of the energy for formation of the cation in the gas phase and, consequently, is a well-defined and direct benchmark for gas-phase electronic structure calculations. Figure 3 shows the valence photoelectron spectrum of **6**. Detailed assignment and discussion of this spectrum will be the subject of a separate paper. Most pertinent for the present purposes is the adiabatic ionization energy, which is the lowest energy ionization from the ground state of the neutral molecule to the geometry-relaxed structure of the positive ion. For large molecules with low-frequency vibrations such as **6**, the adiabatic ionization is not vibrationally resolved, and the adiabatic ionization energy is commonly estimated by extrapolation of the ionization intensity in the region of the ionization onset to the point of zero ionization intensity,[27] which in this spectrum is in the region of 7.5 eV. The electronic structure calculations yield a value of 7.50 eV for the adiabatic ionization energy,

(27) For very large distortions of the positive ion away from the vibrational amplitudes of the neutral molecule, adiabatic ionization intensity may not be observed and the onset of ionization intensity represents an upper bound to the true adiabatic ionization energy.

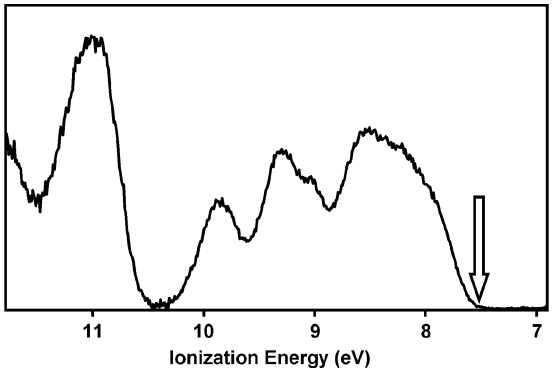

Figure 3. He I gas-phase photoelectron spectrum of **6**. The arrow marks the adiabatic ionization energy obtained by the electronic structure calculations, which compares well with the ionization intensity onset in the spectrum.

which, as the arrow in Figure 3 shows, is in excellent agreement with the onset of ionization intensity in the experimental spectrum.

A significant point from these calculations is the substantial geometrical reorganization that occurs with oxidation and reduction (shown later) of this molecule. Shown below is a comparison of the calculated geometries for the neutral molecule **6** and the cation $\mathbf{6}^+$. The vertical ionization energy, calculated

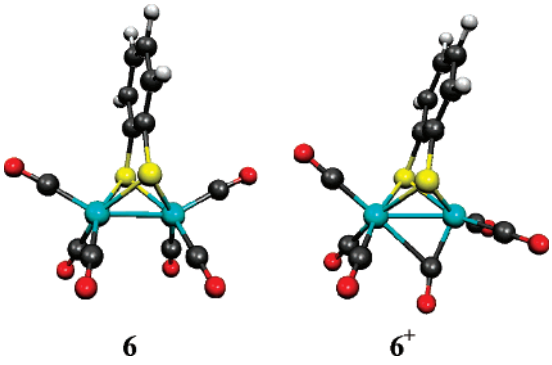

6 $\mathbf{6}^+$

for **6** without a change in geometry, is 0.6 eV higher in energy than the adiabatic ionization energy to $\mathbf{6}^+$, showing the appreciable stabilization of the higher oxidation state $\mathbf{6}^+$ gained from the geometric reorganization energy. In the cation one carbonyl has moved to a semibridging position such that the iron atom on the right side of $\mathbf{6}^+$ in the displayed orientation now has an inverted square-based pyramid ligand arrangement relative to the original orientation. This geometry approximates the hydrogenase enzyme structure shown schematically in **1** with an apparently vacant coordination site on the inverted Fe atom. Such a structure has been the goal of a number of synthetic pursuits.[5] Darensbourg has recently investigated a related molecule shown schematically as **7**, where NHC is an N-heterocyclic carbene.[28] This molecule shows a fully reversible, one-electron oxidation in acetonitrile, and the cation $\mathbf{7}^+$ was isolated and structurally characterized as the PF_6^- salt. The

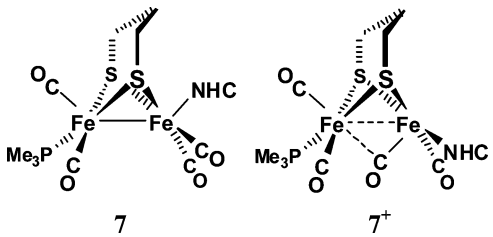

7 $\mathbf{7}^+$

Scheme 1. Procatalyst Initiation and ECEC Mechanism for Catalytic Reduction of Protons to H_2

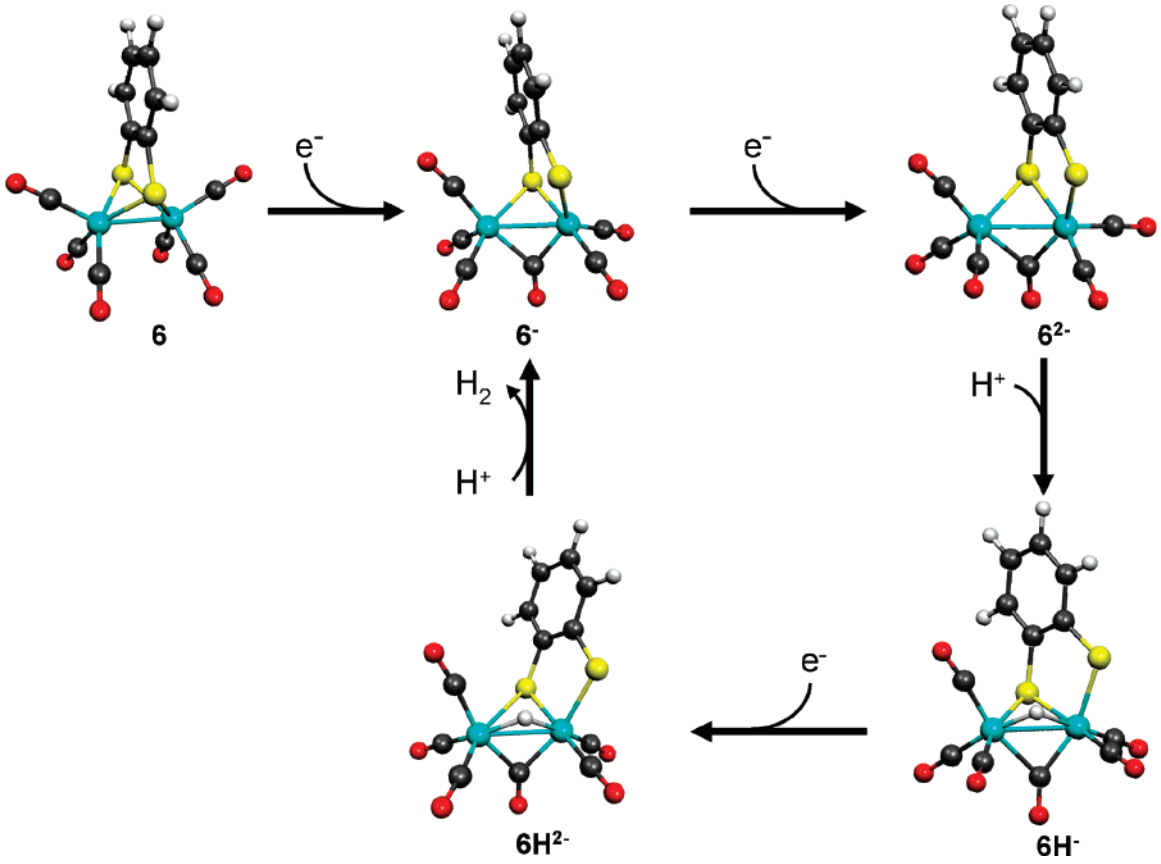

calculated structure of $\mathbf{6}^+$ is analogous to that of $\mathbf{7}^+$, in which both cations have an "inverted" Fe atom and a semibridging carbonyl as shown schematically for $\mathbf{7}^+$. Oxidation of **6** in acetonitrile (not shown) was only quasi-reversible and not pursued further. Also significant in the calculated structure of the cation $\mathbf{6}^+$ is the bending of the bdt ligand toward the Fe atom with the inverted structure, reminiscent of the "dithiolate fold effect" that stabilizes the oxidation states of high-valent early transition metals.[16−19] The agreement between the calculated and experimental adiabatic ionization energies of **6** depends on the ability of the computations to model the reorganization energy associated with the structural changes, and the structure of the cation is consistent with that observed for $\mathbf{7}^+$.

The computations also account well for the reduction of **6** in acetonitrile. A key feature observed in the reduction of **6** is the potential inversion. That is, it is easier to reduce $\mathbf{6}^-$ than **6**, resulting in an overall two-electron reduction. Calculations result in $E_1° = -1.52$ V and $E_2° = -1.06$ V corresponding to a 0.46 V potential inversion. The calculated $E_{ov}°$ of −1.29 V is in good agreement with the observed value of −1.32 V. By simulation of the experimental voltammograms we find that the potential inversion must exceed about 150 mV. For THF solvent, we found by experiment $E_1° = -1.485$ V and $E_2° = -1.500$ V; that is, there was no potential inversion. This type of solvent effect has been attributed to the larger donor number of THF compared to acetonitrile.[29] This large degree of predicted inversion in acetonitrile is indicative of a significant structural change accompanying the electron-transfer reaction.[23] The calculations show a lengthening of one of the Fe−S bonds from 2.28 Å in **6** to 3.33 Å in the anion and movement of a CO to a bridging position (see Scheme 1). In dianion $\mathbf{6}^{2-}$, the calculations show complete cleavage of the Fe−S bond to give an open dianion with a bridging CO (see Scheme 1). This structure for $\mathbf{6}^{2-}$ was suggested by McKennis and Kyba[24] who obtained $\mathbf{6}^{2-}$ by sodium reduction of **6**, and the computations support this proposal.

It has been indicated previously that $\mathbf{6}^{2-}$ has a pK_a on the order of 23 or greater and is rapidly protonated by acids including acetic acid.[21] Our calculated structure for $\mathbf{6H}^-$ is shown in Scheme 1 and its calculated pK_a is 22.9, a value consistent with the previous work. The structure of $\mathbf{6H}^-$ features a μ-bridged hydride structure similar to other published results.[30−32] Protonation of $\mathbf{6}^{2-}$ at iron to form a terminal hydride and at sulfur to yield −SH were also studied computationally. The calculated pK_a values for the corresponding acids are 17.6 and 18.1, respectively, showing that these species are less stable than the μ-bridged hydride by Gibbs free energies of 7.3 and 6.7 kcal/mol. Calculations of a species in which a hydride bridges between a sulfur and an iron minimized to the dimetal μ-bridged hydride species shown in Scheme 1. These results contrast with the corresponding protonated species produced in the electrocatalytic mechanism with **2b**, **d**, **3a**, and **4a** with acetic acid, where it is presumed that protonation takes place at a terminal Fe position.[13]

(28) Liu, T.; Darensbourg, M. Y. *J. Am. Chem. Soc.* **2007**, *129*, 7008−7009.
(29) Barriere, F.; Geiger, W. E. *J. Am. Chem. Soc.* **2006**, *128*, 3980−3989.
(30) Dong, W.; Wang, M.; Liu, X.; Jin, K.; Li, G.; Wang, F.; Sun, L. *Chem. Commun.* **2006**, 305−307.
(31) Ezzaher, S.; Capon, J. F.; Gloaguen, F.; Petillon, F. Y.; Schollhammer, P.; Talarmin, J. *Inorg. Chem.* **2007**, *46*, 3426−3428.
(32) Zampella, G.; Greco, C.; Fantucci, P.; De Gioia, L. *Inorg. Chem.* **2006**, *45*, 4109−4118.

It is reported[21] that protonation of $\mathbf{6H}^-$ is the rate-determining step in the catalytic process with acid. This anion reacts with *p*-toluenesulfonic acid allowing catalytic molecular hydrogen formation but not with the weaker acetic acid. Our observation of a peak for the catalytic reduction of acetic acid near −2.1 V versus ferrocene is ascribed to the reduction of $\mathbf{6H}^-$**.** The calculated value for the standard potential for reduction of $\mathbf{6H}^-$ is −2.05 V versus ferrocene. The calculated structure for $\mathbf{6H}^{2-}$ is shown in Scheme 1. In this structure the intact Fe−S bond in $\mathbf{6H}^-$ is lengthened from 2.339 to 2.860 Å in $\mathbf{6H}^{2-}$. In all of the structures calculated in Scheme 1, the Fe−Fe distance remains relatively constant and within the range for a formal bond to be present.

Various protonations of the $\mathbf{6H}^{2-}$ species were investigated computationally. The calculations indicate that protonation of $\mathbf{6H}^{2-}$ by acetic acid in solution (acetonitrile) on the nonbridging sulfur atom or the terminal iron atom of $\mathbf{6H}^{2-}$ requires 19.0 or 16.9 kcal/mol of free energy, respectively. All attempts to protonate the bridging sulfur on $\mathbf{6H}^{2-}$ result in the proton migrating to the terminal Fe atom during geometry optimizations. However, calculations show that a reaction is highly favored in which the hydride of $\mathbf{6H}^{2-}$ reacts directly with acetic acid to produce molecular hydrogen as shown in eq 2.

$$\mathbf{6H}^{2-} + \mathrm{AcOH} \rightleftharpoons \mathbf{6}^- + \mathrm{AcO}^- + \mathrm{H_2} \qquad (2)$$

In a gas-phase calculation the proton carries out a direct electrophilic attack on the hydride of the metal complex $\mathbf{6H}^{2-}$ and proceeds directly to dissociation of the hydrogen molecule from the complex without an energy barrier. This is a fundamental acid−base reaction and, in solution, only requires the additional energy of solvent reorganization. This mechanism may be typical for the production of H_2 from metal hydrides that are highly basic.[33] The calculated solution free energy favors the H_2 production in eq 2 by −5.03 kcal/mol, and the equilibrium constant for eq 2 is 4900 M. The $\mathbf{6}^-$ thus produced is immediately reduced to $\mathbf{6}^{2-}$ and proceeds on in the catalytic cycle of Scheme 1. Consequently, $\mathbf{6}^-$ not **6** is the catalyst for this reaction which proceeds by an ECEC mechanism as shown in Scheme 1. Hence compound **6** serves as a procatalyst. This contrasts with **2b**, **d**, **3a**, and **4a** in the presence of acetic acid in which an EECC mechanism was suggested and the Fe(I)−Fe(I) species is the catalyst, and with **2c**, **3b**, and **4b** in which an ECEC or perhaps EC mechanism was suggested.[13]

Best and co-workers[34] studied the electrocatalytic production of H_2 from TsOH catalyzed by phosphido-bridged complex **8**.

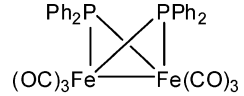

8

Table 2. Reaction Steps and Parameters for Simulation of Electrochemical Results

	$\mathbf{6} + e^- \rightleftharpoons \mathbf{6}^-$	E°_3, $k_{s,3}$, α_3	(3)
	$\mathbf{6}^- + e^- \rightleftharpoons \mathbf{6}^{2-}$	E°_4, $k_{s,4}$, α_4	(4)
rds:[a]	$\mathbf{6}^{2-} + \mathrm{HA} \rightleftharpoons \mathbf{6H}^- + \mathrm{A}^-$	K_5, $k_{f,5}$, $k_{b,5}$	(5)
post-rds:	$\mathbf{6H}^- + e^- \rightleftharpoons \mathbf{6H}^{2-}$	E°_6, $k_{s,6}$, α_6	(6)
post-rds:	$\mathbf{6H}^{2-} + \mathrm{HA} \rightleftharpoons \mathbf{6HH}^- + \mathrm{A}^-$	K_7, $k_{f,7}$, $k_{b,7}$	(7)
post-rds:	$\mathbf{6HH}^- \rightleftharpoons \mathbf{6}^- + \mathrm{H_2}$	K_8, $k_{f,8}$, $k_{b,8}$	(8)

[a] Rate-determining step.

The mechanism for this reaction involves reversible $2e^-$ reduction to give dianion $\mathbf{8}^{2-}$, similar to that proposed for **6**. The dianion is then diprotonated to yield $\mathbf{8H_2}$ which does not evolve H_2. Reduction of $\mathbf{8H_2}$ in two $1e^-$ steps affords $\mathbf{8H_2}^{2-}$ which eliminates H_2 forming $\mathbf{8}^{2-}$ or adds another H^+ to give $\mathbf{8H_3}^-$ which loses H_2 producing $\mathbf{8H}^-$. This mechanism differs from that suggested for **6** in that $\mathbf{8}^{2-}$ is diprotonated and then reduced further, but for $\mathbf{6}^{2-}$ the monoprotonated $\mathbf{6H}^-$ is not further protonated under our conditions until it is further reduced rendering it more basic. It should be noted that the strong acid TsOH protonates $\mathbf{8H}^-$ whereas only weaker carboxylic acids and phenols are present in our experiments with $\mathbf{6H}^-$. Reduction of **6** in the presence of TsOH has been reported and generates H_2 by protonation of $\mathbf{6H}^-$ without the need for further reduction.

The mechanism shown in Scheme 1 was used to simulate the electrochemical results. The steps of the mechanism are shown in reactions 3 through 8 in Table 2 along with the parameters associated with each step, and the values obtained for the parameters from simulation of the data are shown in Table 3. In our simulations, we have postulated that reaction 5 is the rate-limiting step (rds) in the catalytic cycle comprising reactions 6 through 8. The sum of those reactions is the reduction of HA, $2\mathrm{HA} + 2e^- \rightleftharpoons \mathrm{H_2} + 2\mathrm{A}^-$, whose standard potential represents the least negative value at which catalysis can occur.[25] Reactions 6 through 8, which follow the rate-limiting step, are considered to be fast, as indicated by the calculations. Thus, the exact sequence of protonation and electron transfer after the rds is not known on the basis of the electrochemical simulation. As indicated earlier, calculations support the value of E°_6 that was used in the simulations (computations: −2.05 V; electrochemical simulation: −2.08 V versus ferrocene). In addition, the calculations indicate that attack of $\mathbf{6H}^{2-}$ by HA leads directly to $\mathbf{6}^-$, H_2, and A^- with the calculated free energy change being −5.03 kcal/mol (K_{298} = 4900 M). Software limitations preclude inclusion of this reaction as written so it was replaced by reactions 7 and 8, both considered to be fast. The combined equilibrium constant for reactions 7 and 8, K_7K_8, was set equal to 4900 M, as calculated.

The proposed reaction scheme comprising reactions 3 through 8 is quite unusual in that the catalytic reduction peak grows in at a potential where the catalyst **6** shows no reduction peak. Such behavior has recently been observed for a few other hydrogenase mimics.[3,36,37] In fact, **6** is an example of a procatalyst that is first reduced to form the actual catalyst, $\mathbf{6}^-$, which is the species that participates in the catalytic cycle described by reactions 4 through 8. It enters the cycle via reaction 3 and is regenerated in reaction 8.

(33) Although calculations show that reaction of $\mathbf{6H}^{2-}$ with AcOH is facile, it has been reported that a μ-H in a Fe-only hydrogenase model with two Fe(II) centers is experimentally unreactive to HOTf or $H(OEt_2)_2BAr^F{}_4$ in contrast to its terminal hydride isomer: van der Vlugt, J. I.; Rauchfuss, T. B.; Whaley, C. M.; Wilson, S. R. *J. Am. Chem. Soc.* **2005**, *127*, 16012−16013.

(34) Cheah, M. H.; Borg, S. J.; Bondin, M. I.; Best, S. F. *Inorg. Chem.* **2004**, *43*, 5635−5644. See also Cheah, M. H.; Borg, S.J.; Best, S. F. *Inorg. Chem.* **2007**, *46*, 1741−1750.

(35) Izutsu, K. *Acid-Base Dissociation Constants in Dipolar Aprotic Solvents*; Blackwell Scientific Publishers: Oxford, U.K., 1990.

(36) Gloaguen, F.; Lawrence, J. D.; Rauchfuss, T. B.; Benard, M.; Rohmer, M. M. *Inorg. Chem.* **2002**, *41*, 6573−6582.

(37) Windhager, J.; Rudolph, M.; Bräutigam, S.; Görls, H.; Weigand, W. *Eur. J. Inorg. Chem.* **2007**, 2748−2760.

Table 3. Simulation Parameters for Scheme 1[a]

number	reaction	$E°$/V	k_s/cm s^{-1}	α
(3)	$\mathbf{6} + e^- \rightleftharpoons \mathbf{6}^-$	−1.33	1	0.5
(4)	$\mathbf{6}^- + e^- \rightleftharpoons \mathbf{6}^{2-}$	−1.31	1	0.5
(6)	$\mathbf{6H}^- + e^- \rightleftharpoons \mathbf{6H}^{2-}$	−2.08	10	0.5

number	reaction	K	k_f	k_b
(5)	$\mathbf{6}^{2-} + HA \rightleftharpoons \mathbf{6H}^- + A^-$	2	1.0×10^5 M^{-1} s^{-1}	5.0×10^4 M^{-1} s^{-1}
(7)	$\mathbf{6H}^{2-} + HA \rightleftharpoons \mathbf{6HH}^- + A^-$	490	1.0×10^{10} M^{-1} s^{-1}	2.0×10^7 M^{-1} s^{-1}
(8)	$\mathbf{6HH}^- \rightleftharpoons \mathbf{6}^- + H_2$	10 M	1.0×10^{10} s^{-1}	1.0×10^9 M^{-1} s^{-1}
HC[b]	$HA + A^- \rightleftharpoons HA_2^-$	1000	1.0×10^8 M^{-1} s^{-1}	1.0×10^5 s^{-1}

[a] Diffusion coefficients for **6**, $\mathbf{6}^-$, $\mathbf{6}^{2-}$, $\mathbf{6H}^-$, $\mathbf{6H}^{2-}$, and $\mathbf{6HH}^-$ set equal to 1.4×10^{-5} cm^2/s. Diffusion coefficients: HA and A^-: 3.3×10^{-5} cm^2/s; H_2: 4.0×10^{-5} cm^2/s; HA_2^-: 2.0×10^{-5} cm^2/s. Potentials are reported with respect to the ferrocene/ferrocenium couple in acetonitrile. Solution resistance compensated electronically (140 Ω). Electrode area = 0.076 cm^2. $K_5 = 2$ corresponds to $pK_{a,2}(\mathbf{6H_2}) = 22.6$ as $pK_a(CH_3COOH) = 22.3$. The same parameter values were found to fit data obtained with 0.5 mM and 2.0 mM catalyst. [b] Homoconjugation reaction. The reaction rate was assumed to be close to that for a diffusion-controlled reaction. A typical homoconjugation equilibrium constant was taken.[35]

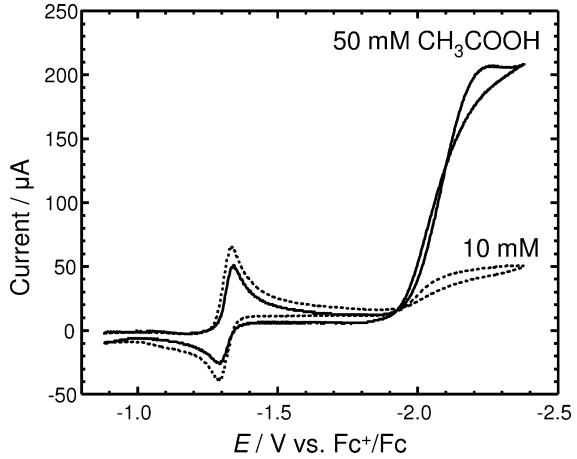

Figure 4. Intentional addition of acetate suppresses catalysis, indicating the presence of acetate in the rate-determining step. Voltammograms of 1.0 mM **6** in 0.10 M $Bu_4N(CH_3CO_2)$, 0.10 M Bu_4NPF_6 in acetonitrile. Scan rate: 0.100 V/s. Acetic acid concentration as indicated.

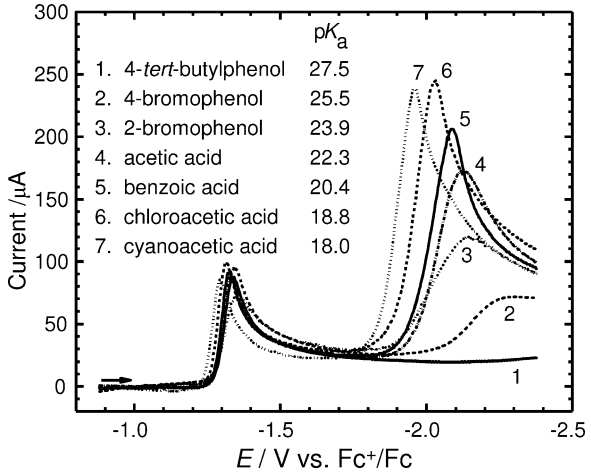

Figure 5. Voltammograms of ca. 1 mM **6** in the presence of 5.0 mM of various acids. Scan rate: 0.100 V/s. pK_a values from Izutsu.[35] In that reference, two values are given for chloroacetic acid, 18.8 (used here) and 15.34.

Figure 1B presents simulations based on reactions 3 through 8 with the simulation parameters listed in Table 3. The same simulation parameters were used for all four concentrations of added acetic acid. The height of the catalytic peak is well accounted for by the simulations, but there are noticeable differences in the peak shape and position. An important feature in the experimental voltammograms (arrow, Figure 1A) is the suppression of the oxidation peak for $\mathbf{6}^{2-}$ (near −1.3 V) as the concentration of acetic acid is increased. Reproducing this suppression allowed estimation of $K_5 = 2$ from the simulations in Figure 1B. When K_5 is less than 2, the simulated peak for oxidation of $\mathbf{6}^{2-}$ is too large. When it is greater than 2, the peak is too small because more of $\mathbf{6}^{2-}$ is converted to $\mathbf{6H}^-$ in the simulation and $\mathbf{6H}^-$ is not oxidized at this potential. A less negative potential is required for oxidation.[21]

The rate-determining step, reaction 5, has acetate ion as a product. Thus, it is expected that intentional addition of acetate ion will suppress the rate of catalysis. Alternatively viewed, the acetate ion acts as a base and deprotonates $\mathbf{6H}^-$ as would any other base of comparable or greater basicity. In Figure 4, voltammograms are shown for 1 mM **6** and 10 and 50 mM acetic acid in 0.10 M Bu_4NPF_6 plus 0.10 M $Bu_4N(CH_3CO_2)$. For 50 mM acetic acid, the catalytic current is only about 200 μA, five times smaller than that in the absence of added acetate (Figure 1). A similar suppression is seen for 10 mM acetic acid.[38] In addition, the catalytic process is not peak-shaped in the presence of acetate. It adopts a sigmoidal shape that is characteristic of a chemical reaction preceding the electrode reaction (CE mechanism) where the current is largely controlled by the rate of the preceding chemical reaction, reaction 5.[39] Simulations of the voltammograms in the presence of added acetate and using the parameters in Table 3 produced catalytic currents close to those observed in Figure 4.

As the equilibrium and rate of reaction 5 are of crucial importance in governing the catalytic current, we investigated acids that are weaker than acetic acid as well as some that are stronger. Results for 1 mM **6**, 5 mM acid, and 0.10 V/s are shown in Figure 5. The conjugate base of the acids was not added in these experiments. For the sake of clarity, only the forward scans are shown. With the weakest acid, 4-*tert*-butylphenol, no catalytic current is discernible, but as the acid strength[35] is increased in the order 4-bromophenol < 2-bromophenol < acetic < benzoic, there is a corresponding increase in the catalytic current. Finally for the strongest of the acids,

(38) Compound **6** is not stable in the presence of acetate alone with decomposition occurring over a period of a few minutes. The presence of acid slows the decomposition. The data shown in Figure 4 were obtained by adding 10 mM acetic acid to the solution containing 0.100 M acetate. Then the catalyst was added, and the voltammogram was recorded. The acetic acid concentration was then increased to 50 mM. We suspect that the smaller peak height for catalyst reduction seen with 50 mM is due to some decomposition that occurred between recording the 10 and 50 mM voltammograms.

(39) Bard, A. J.; Faulkner, L. R. In *Electrochemical Methods: Fundamentals and Applications*; Wiley: New York, 2001; pp 488−496.

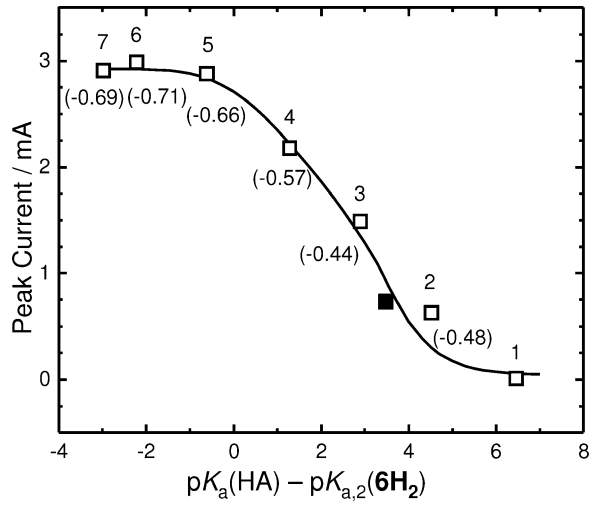

Figure 6. Points: Catalytic peak current for 1 mM **6**, 50 mM acid and 1.00 V/s. Acid numbers same as those in Figure 5. Filled symbol: 1,1,1,3,3,3-Hexafluoro-2-propanol. In parentheses: Overpotentials as discussed in the text. Curve: Digital simulations using the parameter values in Table 3 but with $k_{f,5} = 10^6$ M^{-1} s^{-1} and variable K_5. pK_5 = pK_a(HA) − p$K_{a,2}$(**6H$_2$**). p$K_{a,2}$(**6H$_2$**) = 21 provides the best average fit to the data for the seven acids studied at 50 mM.

chloroacetic and cyanoacetic acid, the catalytic peak reaches a limiting value. This limit corresponds to catalysis of such high efficiency that the peak current is actually controlled by the diffusion of the acid to the electrode. That is, the catalytic cycle is no longer rate-limiting. This point will be discussed in more detail later. Eventually, with acids as strong as *p*-toluenesulfonic acid (pK_a = 8.7 in acetonitrile) moderate catalysis is seen at the first reduction peak as reported by Capon et al.[21]

Small changes in the first reduction peak are also seen. Part of the variation in this peak height stems from concentration differences. The concentration of **6** ranged from 1 to 1.04 mM for this series. For the stronger acids, there is a shift in the peak potential in the positive direction which can be traced to protonation of **6**$^{2-}$ to form **6H**$^-$. This qualitative trend is matched by simulation.

To interpret the dependence of the catalytic peak height on pK_a, we conducted simulations using the same parameters as those in Table 3 except that K_5 was varied from 10^{-7} to 10^3 and $k_{f,5}$ was maintained at 10^6 M^{-1} s^{-1} except for those values of K_5 which were so small that $k_{b,5}$ would have exceeded 10^9 M^{-1} s^{-1}, taken as an estimate of the diffusion-controlled limit. In this range $k_{f,5}$ was lowered accordingly in order to keep $k_{b,5}$ at 10^9 M^{-1} s^{-1}. The simulations were conducted for 50 mM acid, 1 mM **6**, and 1.00 V/s. The simulated catalytic peak current was measured from the simulated value in the absence of acid. The results are shown in Figure 6. Also shown in Figure 6 are the experimental peak currents, measured from the zero-acid baseline, as were the simulations. The numbering of the acids is the same as that in Figure 5. The abscissa is the difference between the pK_a of the acid and that of the acid dissociation constant of **6H**$^-$, p$K_{a,2}$(**6H$_2$**). The value of the latter was adjusted to bring the simulated curve into approximate congruence with the experimental data, which required p$K_{a,2}$(**6H$_2$**) = 21 (or 22.6 from studies of acetic acid alone; see footnote of Table 3). Thus the acidity of **6H**$^-$ obtained by proton-transfer equilibrium postulated in reaction 5 and evaluated by simulation is quite consistent with the calculated pK_a 22.9.

Also included in Figure 5 is the data point for 1,1,1,3,3,3-hexafluoro-2-propanol (filled symbol). As the pK_a of this acid is not known in acetonitrile, we adjusted it to bring that data point close to the simulated curve resulting in a pK_a value of 24.5.

In carrying out the simulations in Figure 6, we were able to gain insight into the rate of catalysis. In the plateau region corresponding to the stronger acids (acids 5−7), examination of the simulated concentrations in the diffusion-kinetic layer near the electrode at the peak potential of the catalytic process revealed that the surface concentration of the acid was only 1−2% of its concentration in the bulk. This means that, in this limit, the current is controlled by the diffusion of the acid. The catalytic cycle is sufficiently fast that it is not rate-determining for these acids. Simulations for 2-bromophenol (acid 3), however, showed that the surface concentration was about 50% of the bulk concentration indicating a current that is in part controlled by the rate of the catalytic cycle.

The data clearly show that the catalyst is less effective with weaker acids. However, as the acids become weaker, the standard potential for reduction of the acid, $E°_{HA}$, moves in the negative direction[25] so the overpotential for the catalytic reduction might be smaller than that with stronger acids. This trend was confirmed by measuring the overpotential as the difference between the standard potential and the half-peak potential for the data in Figure 5. The resulting overpotential values are shown in parentheses near each data point in Figure 6. As one can see, the values range from a high of about −0.7 V to a low of about −0.45 V with the trend being that the weaker acids are reduced with lower overpotential. A practical catalyst should operate at the lowest possible overpotential. However, for the present case this lowering of the overpotential comes at a price of severely suppressed catalytic activity. We are not certain if this is a general result or if it is specific to this catalyst.[40] However, we note that the biological catalysts, Fe-only hydrogenases, produce molecular hydrogen with exceptionally high turnover rates and low overpotential.

The concentration dependence of the catalytic current is shown for two acids in Figures 7 and 8. For cyanoacetic acid, at concentrations below about 10 mM and at the smallest scan rate, the reaction is close to being diffusion-controlled, meaning that the catalytic cycle is fast enough so as not to be rate-limiting. A catalytic peak whose magnitude is controlled by the diffusion of acid should increase linearly with acid concentration. One can see that this is approximately true at low concentrations and low scan rates (see lines in Figure 7). However, the available (or potential) flux of the acid to the reaction layer is proportional to $c_{HA}\upsilon^{1/2}$ where c_{HA} is the concentration of added acid and υ is the scan rate.[39] Thus, as the concentration and/or the scan rate is increased, the available flux increases such that the catalytic rate becomes partially controlled by the rate of the catalytic cycle and the observed

(40) The results of simulations reported in Figure 5 are for the catalytic peak current only. As seen in Figure 6, another feature of the data is that the peak potential moves in the positive direction as the acid strength increases. The simulated peak potentials, however, are almost independent of acid strength, based on reactions 3 through 8. There are various other reactions that will cause a potential shift similar to that seen in Figure 6. For example, formation of a hydrogen-bonded complex between **6H**$^-$ and A$^-$ (**6H**$^-$·A$^-$) or between **6H**$^{2-}$ and HA (**6H**$^{2-}$·HA) will have the effect of shifting the peak if one assumes that the formation constants correlate with acid strength. As there are many such possible reactions, and perhaps other types as well, we have refrained from attempting to fit this potential shift.

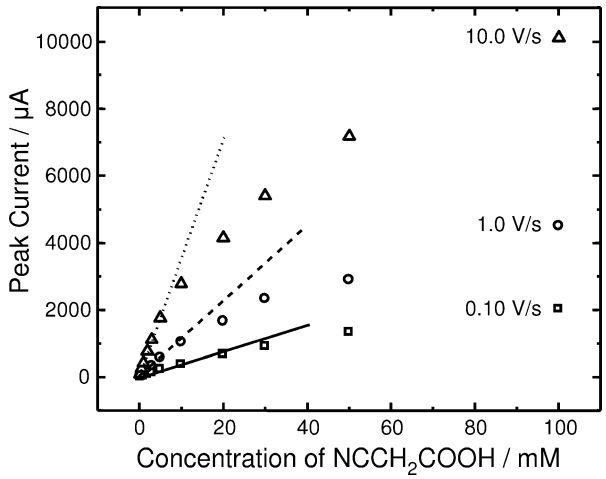

Figure 7. Dependence of the catalytic peak current for 1.0 mM **6** on concentration of cyanoacetic acid and scan rate. Lines: Currents controlled by diffusion of cyanoacetic acid (solid: 0.10 V/s; dashed: 1.0 V/s; dotted: 10.0 V/s).

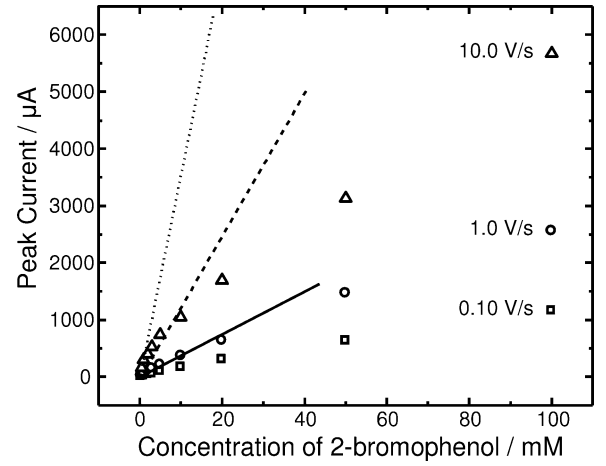

Figure 8. Dependence of the catalytic peak current for 1.0 mM **6** on concentration of 2-bromophenol and scan rate. Lines: same as those drawn in Figure 7.

currents are smaller than those predicted by extrapolation of the low-concentration/low-scan rate lines. Notice that the deviation from linearity occurs at higher concentrations for 0.10 V/s compared to the higher scan rates. The slopes of the lines correspond to diffusion-controlled conditions where the current is proportional to $v^{1/2}$. For 2-bromophenol (Figure 8), the reaction is under partial control by the catalytic cycle at virtually all scan rates and concentrations. In the pure kinetic region[39] the reduction would produce a perfectly flat plateau and the plateau current would be independent of scan rate.[39] None of the acids studied here fell into this pure kinetic region. Peak current−concentration data for other acids are provided in the Supporting Information.

In summary, we report that electrochemical generation of dihydrogen from weak acids catalyzed by [μ-(1,2-benzenedithiolato)][$Fe(CO)_3$]$_2$, **6**, occurs by a novel mechanism deduced from electrochemical and computational studies. This catalysis occurs at a potential where the catalyst itself shows no electroactivity. The kinetics and overpotentials of dihydrogen production have been systematically investigated for the first time.

Experimental Section

Compound **6** was prepared as described earlier[26] and identified by the IR spectrum (Figure 2) collected on a Nicolet 380 FT-IR spectrophotometer. Photoelectron spectra were recorded using an instrument that features a 36 cm radius, a 8 cm gap hemispherical analyzer[41] with a custom-designed photon source, sample cells, digital electronics, and control software as described previously.[42] Calibration of the ionization energy scale was carried out using the $^2P_{3/2}$ ionization of argon (15.759 eV) and the $^2E_{1/2}$ ionization of methyl iodide (9.538 eV), and the spectrometer drift was controlled to less than ±0.005 eV using the argon $^2P_{3/2}$ peak as an internal calibration lock of the absolute ionization energy. The instrument resolution, measured using the full width at half-maximum of the argon $^2P_{3/2}$ ionization during actual data collection, was 0.022−0.029 eV. The sample sublimed cleanly in the 10^{-4} Torr pressure vacuum, and data were collected in the range 45−85 °C with no visible changes in the spectra during data collection. At 95 °C decomposition began as evidenced by the appearance of free CO in the spectrum, but no other volatile species were observed. The spectrum is corrected for the He Iβ line (1.866 eV higher in energy and 3% the intensity of the He Iα line) present in a He discharge source and for the change in instrument analyzer sensitivity as a function of the electron kinetic energy.

For the electrochemical experiments, all acids and tetrabutylammonium acetate were of commercial origin and were used as received. The source and treatment of the solvent and supporting electrolyte have been described earlier.[23] All experiments were conducted in acetonitrile with 0.10 M tetrabutylammonium hexafluorophosphate (Bu_4NPF_6) as supporting electrolyte. Electrodes, cells, instrumentation, and electrochemical procedures have been described.[23] In the present study the potentiostat was an EG&G PAR model 273. The working electrode was a mercury film on gold disk electrode prepared as described earlier.[25] Its area was 0.076 cm^2, ascertained by studies of the oxidation of ferrocene whose diffusion coefficient is known.[23] Evaluation of solution resistance was carried out as described earlier,[23] and the resistance was compensated by electronic resistance compensation. The laboratory reference electrode was a silver wire in contact with 0.010 M $AgNO_3$, 0.10 M Bu_4NPF_6, acetonitrile (AgRE). Its potential was frequently measured with respect to the reversible ferrocene/ferrocenium couple, in acetonitrile, and all potentials are referred to ferrocene. Voltammetric experiments were carried out at 298 K, and the electolyses were done at room temperature.

The voltammetric cell included a platinum wire counter electrode immersed in the test solution. A reviewer has suggested that there is a danger that platinum may anodically dissolve from the counter electrode and redeposit in the mercury film working electrode. As platinum will catalyze the direct reduction of the acids, it was felt that the results might have been compromised by this platinum crossover. We carried out cyclic voltammetry experiments with 10 mM acetic acid in acetonitrile using a glassy carbon counter electrode and a mercury-film working electrode. A total of 40 scans, including the potential where significant hydrogen was produced, were recorded at 0.10 V/s. The glassy carbon counter electrode was then replaced by the platinum wire counter electrode, and the experiment was repeated. No change in the overpotential for reduction of acetic acid was observed. These experiments, requiring about 20 min for each, indicate that any such platinum crossover has a negligible effect on the hydrogen overpotential at our mercury film electrode, which is in line with the inert nature of the platinum counter electrode. Crossover in the electrolysis cell is even more unlikely as the counter electrode is situated in a separate compartment.

(41) Siegbahn, K.; Nordling, C.; Fahlman, A.; Nordberg, R.; Hamrin, K.; Hedman, J.; Johansson, G.; Bergmark, T.; Karlsson, S. E.; Lindgren, I.; Lindberg, B. *Nova Acta Regiae Societatis Scientiarum Upsaliensis* **1967**, *20*, 282.
(42) Lichtenberger, D. L.; Kellogg, G. E.; Kristofzski, J. G.; Page, D.; Turner, S.; Klinger, G.; Lorenzen, J. *Rev. Sci. Instrum.* **1986**, *57*, 2366.

Controlled potential electrolysis was performed in an airtight cell with either a platinum mesh (ca. 15 cm^2 projected area) or a mercury pool working electrode (ca. 40 cm^2), a platinum wire counter electrode, separated from the working electrode compartment by a medium porosity glass frit, and the AgRE. Stirring was accomplished with a magnetic stirbar. At sufficiently high currents, bubbles may be seen to form on the electrode surface during voltammetry (Supporting Information), and they may possibly block part of the surface. When the bubbles spontaneously detach from the surface, the resulting stirring causes erratic bumps and spikes in the current−potential curve.

Controlled potential coulometry of **6** in acetonitrile with no added acid required approximately two electrons per molecule of **6**. However, the charge−time curve did not reach a plateau, and voltammetry of the electrolyzed solution revealed that much of the expected $\mathbf{6}^{2-}$ was missing. A similar result was reported by Capon et al.[21]

We measured the turnover number by electrolysis of 10 mM acetic acid in the presence of 1 mM **6** in acetonitrile at a mercury-pool electrode. After about 30 min the charge passed was equivalent to reduction of all of the acetic acid. The charge due to direct reduction of acetic acid at the working electrode was less than 2% of the total charge. Only 14% of the catalyst system remained at the end of the electrolysis which corresponds to a turnover number of ∼11 (mol acetic acid reduced/mol of catalyst before deactivation). After electrolysis under an argon atmosphere the overhead gas was analyzed by GC[43] and the predominant species detected was identified as molecular hydrogen.

Somewhat cleaner electrolyses in the absence of added acid were obtained in dichloromethane with 0.50 M Bu_4NPF_6. Here the charge−time curve reached a plateau (electrolysis current approached zero) corresponding to a two-electron reduction. However, voltammetric analysis of the solution showed that most of the expected $\mathbf{6}^{2-}$ was absent. Electrolyses in either acetonitrile or dichloromethane in the absence of light gave similar results to those for electrolyses conducted under ordinary room lighting.

Digital simulations were conducted with DigiElch, version 2.0, a free software package for the **Digi**tal simulation of common **El**ectro-**ch**emical experiments (http://www.digielch.de).[44] The fitting routine in that program was used to establish the final best-fit parameter values for many of the variables.

All computations were performed with ADF2006.01b.[45−47] Geometry optimizations and frequency calculations were carried out using the VWN functional with the Stoll correction implemented.[48] Figures of the optimized geometries were created with the program Molekel.[49] All electronic energies reported were calculated using the OPBE density functional.[50] Recent comparisons of OPBE to other common functionals found it to be the best for the prediction of nuclear magnetic constants[51] and the only functional to correctly predict the spin states of seven different iron complexes.[50] Our comparisons with other common functionals in the ADF package have also shown it to be among the best at predicting the oxidation and reduction potentials of several iron complexes and the pK_a's of the acids included in this study. A triple-ζ STO basis set with one polarization function (TZP), available in the ADF package, was used in all calculations. Relativistic effects were taken into account in all calculations by using the scalar ZORA formalism[52] implemented as part of the ADF2006.01b program. All electronic structures with unpaired spins were calculated using an unrestricted framework. Only low-spin complexes have been analyzed.

The theoretical stretching frequencies for all species were calculated analytically with the same DFT model as that for the geometry optimization, and the lack of imaginary frequencies shows that each geometry is a true minimum. For comparison of the calculated gas-phase CO frequencies with the experimental solution frequencies for compound **6**, the calculated frequencies were shifted lower by 55 cm^{-1}. This corresponds to a scaling of CO frequencies from calculated to experiment by a factor of ∼0.98. Because the adjustment in the calculated frequencies is small, and because the thermal contribution to the free energies for redox potentials and pK_a's is a small contribution to the total values, the vibrational frequencies were used unchanged in the calculations of the free energies in the catalytic scheme. For visual comparison of the simulated IR spectrum with the experimental IR spectrum of **6**, the calculated absorptions were broadened with a Gaussian function as in previous work.[53] The two absorptions calculated at higher frequency were broadened by 7 cm^{-1}, and the lower frequency absorptions were broadened by 10 cm^{-1} to nominally approximate the broadening that is observed.

Solvation effects on the complexes were modeled through the Conductor-like Screening Model (COSMO) of solvation.[54] The solvent parameters implemented were those defined by the ADF2006.01b program to simulate an acetonitrile solvated environment. Free energy (G) values were calculated from the electronic self-consistent-field (SCF) energies considering the $q_{translational}$, $q_{rotational}$, and $q_{vibrational}$ contributions.[55] Enthalpy and entropy terms were calculated under standard temperature and pressure.

Standard potentials versus ferrocene were computed as the free energy difference of the reaction $Fc + A \rightleftharpoons Fc^+ + A^{\bullet -}$ (all solvated), where A is the diiron complex under investigation. From this, the standard potential is obtained by the relation $E°_{A/A^{\bullet -}}$ vs ferrocene $= -\Delta G°_{rxn}/F$ where F is Faraday's constant. The absolute half-cell potential for the Fc/Fc^+ couple was calculated to be −5.00 V in acetonitrile, which is in good agreement with the −5.05 value estimated from analysis of the surface dipole problem.[56] When computing K_a values, the proton was treated as having one molecule in the primary solvation sphere, CH_3CN-H^+, and this species was considered to participate in the reaction, $HA + CH_3CN \rightleftharpoons A^- + CH_3CN-H^+$, in a solvated environment.

Acknowledgment. The support of the National Science Foundation through the Collaborative Research in Chemistry program, Grant No. CHE 0527003, is gratefully acknowledged.

Supporting Information Available: Plots of catalytic peak current for three different scan rates as a function of the concentration of seven other acids as well as voltammograms of **6** and acetic acid using a glassy carbon working electrode. Pictures showing bubbles of hydrogen formed during voltammetry of **6** in the presence of acetic acid. Cartesian coordinates of calculated complexes. Structures of less thermodynamically favorable protonated species. This material is available free of charge via the Internet at http://pubs.acs.org.

JA073886G

(43) Valenty, C. *J. Anal. Chem.* **1978**, *50*, 669−670.
(44) Rudolph, M. *J. Electroanal. Chem.* **2003**, *543*, 23−29.
(45) Guerra, C. F.; Snijders, J. G.; Te Velde, G.; Baerends, E. J. *Theor. Chem. Acc.* **1998**, *99*, 391−403.
(46) te Velde, G.; Bickelhaupt, F. M.; Baerends, E. J.; Fonseca Guerra, C.; van Gisbergen, S. J. A.; Snijders, J. G.; Ziegler, T. *J. Comput. Chem.* **2001**, *22*, 931−967.
(47) ADF2006.01b, SCM, Theoretical Chemistry, Vrije Universiteit, Amsterdam, The Netherlands, 2006, *http://www.scm.com*.
(48) Stoll, H.; Pavlidou, C. M. E.; Preuss, H. *Theor. Chim. Acta* **1978**, *49*, 143−149.
(49) Portmann, S.; Luthi, H. P. *Chimia* **2000**, *54*, 766−769.
(50) Swart, M.; Ehlers, A. W.; Lammertsma, K. *Mol. Phys.* **2004**, *102*, 2467.
(51) Zhang, Y.; Wu, A.; Xu, X.; Yan, Y. *Chem. Phys. Lett.* **2006**, *421*, 383−388.
(52) van Lenthe, E.; Ehlers, A.; Baerends, E. *J. Chem. Phys.* **1999**, *110*, 8943−8953.
(53) Borg, S. J.; Tye, J. W.; Hall, M. B.; Best, S. P. *Inorg. Chem.* **2007**, *46*, 384−394.
(54) Klamt, A. *J. Phys. Chem.* **1995**, *99*, 2224−2235.
(55) Jensen, F. *Introduction to Computational Chemistry*; Wiley: Chichester, U.K., 2002.
(56) Reiss, H.; Heller, A. *J. Phys. Chem.* **1985**, *89*, 4207−4213.